ORIGINAL ARTICLE - VASCULAR NEUROSURGERY - ANEURYSM

Shape irregularity of the intracranial aneurysm lumen exhibits diagnostic value

Norman Juchler [1,2] • Sabine Schilling [1,3] • Philippe Bijlenga [4] • Sandrine Morel [4,5] • Daniel Rüfenacht [6] •
Vartan Kurtcuoglu [2,7,8,9] • Sven Hirsch [1]

Abstract

Background Morphological irregularity is linked to intracranial aneurysm wall instability and manifests in the lumen shape. Yet there is currently no consent on how to assess shape irregularity. The aims of this work are to quantify irregularity as perceived by clinicians, to break down irregularity into morphological attributes, and to relate these to clinically relevant factors such as rupture status, aneurysm location, and patient age or sex.

Methods Thirteen clinicians and 26 laypersons assessed 134 aneurysm lumen segmentations in terms of overall perceived irregularity and five different morphological attributes (presence/absence of a rough surface, blebs, lobules, asymmetry, complex geometry of the parent vasculature). We examined rater agreement and compared the ratings with clinical factors by means of regression analysis or binary classification.

Results Using rank-based aggregation, the irregularity ratings of clinicians and laypersons did not differ statistically. Perceived irregularity showed good agreement with curvature (coefficient of determination $R^2 = 0.68 \pm 0.08$) and was modeled very accurately using the five morphological rating attributes plus shape elongation ($R^2 = 0.95 \pm 0.02$). In agreement with previous studies, irregularity was associated with aneurysm rupture status (AUC $= 0.81 \pm 0.08$); adding aneurysm location as an explanatory variable increased the AUC to 0.87 ± 0.09. Besides irregularity, perceived asymmetry, presence of blebs or lobules, aneurysm size, non-sphericity, and curvature were linked to rupture. No association was found between morphology and any of patient sex, age, and history of smoking or hypertension. Aneurysm size was linked to morphology.

Conclusions Irregular lumen shape carries significant information on the aneurysm's disease status. Irregularity constitutes a continuous parameter that shows a strong association with the rupture status. To improve the objectivity of morphological assessment, we suggest examining shape through six different morphological attributes, which can characterize irregularity accurately.

Keywords Intracranial aneurysms · Quantitative morphology · Irregularity · Human ratings

---

This article is part of the Topical Collection on *Vascular Neurosurgery - Aneurysm*

✉ Norman Juchler
  norman.juchler@uzh.ch

✉ Sven Hirsch
  sven.hirsch@zhaw.ch

1 Institute of Applied Simulation, Zurich University of Applied Sciences, Wädenswil, Switzerland

2 The Interface Group, Institute of Physiology, University of Zurich, Zurich, Switzerland

3 Institute of Tourism ITW, Lucerne University of Applied Sciences and Arts, Lucerne, Switzerland

4 Neurosurgery Division, Department of Clinical Neurosciences, Geneva University Hospital and Faculty of Medicine, Geneva, Switzerland

5 Department of Pathology and Immunology, Faculty of Medicine, University of Geneva, Geneva, Switzerland

6 Neuroradiology, SNRI, Klinik Hirslanden, Zurich, Switzerland

7 Zurich Center for Integrative Human Physiology, University of Zurich, Zurich, Switzerland

8 National Center of Competence in Research, Kidney.CH, Zurich, Switzerland

9 Neuroscience Center Zurich, University of Zurich, Zurich, Switzerland

Introduction

Intracranial aneurysms (IAs) are focal deformations of cerebral arteries, prevalent in 2–5% of the population. [32] IAs normally remain stable, yet they rupture with a lesion incidence rate of 1.2% per patient-year. [34] The resulting hemorrhagic stroke is catastrophic with high mortality and morbidity. [15, 26] IAs are increasingly detected due to improving imaging technology and its frequent regular use. As most diagnosed IAs are deemed to be stable, clinicians have to take complex disease management decisions. Meanwhile, biomarkers expressing the instability of the detected IA are still lacking today.

Recent studies on the pathogenic processes of wall remodeling suggest that the biological status of the IA manifests in shape changes. Irregularly shaped aneurysms have been associated with instable wall conditions [12, 25] and higher risk of rupture. [16, 20, 31] Morphological wall characteristics such as irregular protrusions, flattened and slightly curly surfaces, or indentations are assumed to indicate destructive remodeling processes within the vessel wall, thrombus formations or vessel wall hyperplasia [12, 17, 25]. IA wall remodeling is thought to be a progressive process, where with further deterioration of the wall more irregularities appear. Hence, radiologists often appraise the shape of the aneurysm lumen as a proxy for wall remodeling.

Aneurysm shape irregularity has recently been added to the risk assessment of IAs. [1, 10, 33] Although used as a descriptive category, shape irregularity is not formally defined, leading to inconsistent shape assessments between raters. [11, 30] A considerable number of metrics exists to quantify IA morphology, [3, 9, 27, 28] but no robust criteria to distinguish between regular and irregular shapes have been established so far.

We have previously developed a quantitative model for lumen irregularity that matches the human perception of shape. [13] We employed a psychometric method to measure the perceived irregularity of IA domes from human raters assessing highly resolved representations of IA lumens. We reproduced aggregated shape assessments accurately by using a multivariate model of quantitative shape features that can be computed automatically from image data.

In this study, we examine the diagnostic value of lumen irregularity in IA domes in three steps: (a) evaluate the consistency of clinical experts and instructed laypeople in their assessment of irregularity; (b) identify the selection of morphological attributes that reflects perceived irregularity best; and (c) determine whether irregularity is associated with the known clinical risk factors aneurysm location, patient's sex, age, smoking status, and history of arterial hypertension, as well as the aneurysm's rupture status.

Materials and methods

Imaging and patient data

Between September 2006 and July 2015, information on 1164 patients was collected prospectively and consecutively in the @neurIST study [4] at the Geneva University Hospital. A significant proportion of the cohort was only followed up using magnetic resonance imaging (MRI) or computed tomography (CT) imaging. A total of 593 patients were identified as being at risk or suffered from a ruptured aneurysm and were therefore investigated by 3D rotational angiography (3DRA). From these cases, we selected 110 patients through a two-stage randomized process (first step: subset of 255 patients for which 3D reconstructions were accessible; second step: subset of 110 patients that visited the clinic between July 2014 and July 2015 for treatment or aftercare), harboring a total of 134 saccular IAs (41 ruptured, 78 unruptured, 15 with uncertain rupture status). In addition to angiographic data, the dataset included sex, age, rupture status (per aneurysm), history of smoking, and history of hypertension for a subset of the patients (Table 1).

We included both ruptured and unruptured aneurysms to compare the morphology between these two subcohorts and to benchmark our findings with existent literature. While the rupture status reflects aneurysm wall instability approximatively, the comparison shall not be overinterpreted as a prediction of the rupture risk.

Morphometric quantification of the IA lumen

For the assessment of the morphology, we extracted geometric 3D models of the aneurysms and the surrounding vasculature from the 3D angiographies by applying vessel lumen segmentation (geodesic active regions [6], implemented in the software package GIMIAS [18] by CISTIB, University of Sheffield).

For the automated radiomic description, we derived quantitative morphometric data for each aneurysm dome. [22, 28] Most notably, we computed aneurysm size (aSz), the non-sphericity index (NSI), and the normalized total Gaussian curvature (GLN). aSz is the maximum diameter of the aneurysm dome. NSI captures elongation and surface undulation of the dome. It assumes values between 0 and 1, where $NSI = 0$ holds for a perfect half-sphere. GLN is a measure for the total Gaussian curvature of the IA dome, normalized by the total curvature of a sphere with equal volume. We employed inhouse software written in Python for these morphological computations, as well as for all subsequent statistical analyses.

Table 1 110 patients harboring 134 aneurysms were included in this study. Smoker—former or current smoker after the estimated consumption of 300 or more cigarettes. Arterial hypertension—blood pressure greater than 140/90 mmHg, independent of any treatment for hypertension. *MCA M1*, M1 segment of the middle cerebral artery; *ICA oph*, ophthalmic segment of the internal carotid artery; *PComA*, posterior communicating artery; *AComA*, anterior communicating artery; *ACA A2-Per*, pericallosal segment of the anterior cerebral artery; *BA tip*, tip of the basilar artery; *ICA bif*, ICA bifurcation; *aSz*, aneurysm size; *AR*, aspect ratio; *NSI*, non-sphericity index; *GLN*, total Gaussian curvature (normalized)

Overview: patients			Unknown
Sex	81 females (age: 54.4y)	29 males (age: 50.6y)	0
Aneurysm rupture status	41 ruptured	56 unruptured	13
Smoking status	57 with smoking history	35 non-smokers	18
Hypertension status	40 with hypertension history	56 without hypertension	14

Overview: aneurysms		ruptured	unruptured	unknown	total
Total		41	78	15	134
Patient sex	female	26	62	10	98
	male	15	16	5	36
Locations	MCA M1	5	25	2	32
	ICA oph	3	16	4	23
	PComA	10	9	4	23
	AComA	11	8	1	20
	ACA A2-Per	2	5	1	8
	BA tip	3	4	0	7
	ICA bif	0	5	1	6
	others	7	6	2	15
Size/Shape	aSz [mm]	8.6±3.9	6.3±3.1	6.2±2.2	7.0±3.4
(mean±std)	AR [-]	1.5±0.5	1.1±0.4	1.2±0.6	1.2±0.5
	NSI [-]	0.21±0.06	0.13±0.06	0.15±0.10	0.16±0.07
	GLN [-]	6.9±3.2	4.2±1.9	5.1±3.1	5.1±2.8

Morphological assessment of IA lumen by human raters

A total of 39 raters were included in this study: 13 *clinical experts* with an average experience of 12.0 years in researching or treating IAs, 26 *instructed laypersons* with a biological or technical background and at least a general understanding of the disease.

The raters assessed each IA in terms of shape irregularity on a 9-point rating scale, from "1—very regular" to "9—very irregular." The task description emphasized the subjective assessment of shape. No clinical information on the cases was provided. A subset of 26 participants (10 clinical experts, 16 instructed laypersons) assessed the presence/absence of five *morphological attributes* for each IA: rough (non-smooth) surface, blebs, lobules, asymmetric appearance, complex configuration of the parent vasculature/bifurcation, or none of these.

To aggregate the ordinal irregularity ratings per aneurysm, we ranked the rating data per rater (to adjust for rater bias) and computed the means per case, normalized to the range [0, 1]. For the binary ratings of the morphological attributes, we computed the number of votes in favor of that attribute, normalized by the total number of assessments for that case. All rating aggregates p'_{ik}, for aneurysm i and attribute k, take on values between 0 and 1, the limits standing for "very weakly perceived" and "very strongly perceived," respectively. We refer to these metrics p'_{ik} as *perceived* (e.g., perceived irregularity, perceived asymmetry).

We examined the consistency of the ratings as follows. For the *ordinal* irregularity ratings, we calculated the mean Spearman rank correlation between perceived irregularity of the entire cohort and the corresponding ratings computed per rater. For the *binary* attribute ratings, we computed Cohen's kappa between each rater and the individually binarized average rater.

Missing *rating* data was handled by exclusion. Our method is generally robust with respect to missing or outlying rating data. [13] Missing *clinical* data was also handled by exclusion, under the assumption that the misses occurred at random and independent of the property under examination. The numbers of valid cases per property are reported in Table 2.

Relationship between irregularity and morphological attributes

We assessed the relationship of the morphological attributes with perceived irregularity both univariately and multivariately. We applied 5-fold cross-validated, ordinary least squares regression, for which we report the coefficient

Table 2 Morphological attributes, aneurysm size (aSz), non-sphericity (NSI), total curvature (GLN), and patient age (green columns) and their relationship to binary or binarized factors (blue columns) and scalar factors (red columns). Relative frequency (RF): number of times a (binary) attribute was identified divided by the number of cases and raters. Rater agreement for binary assessments is given as the mean Cohen's κ between the rater and the individually binarized average rater, and as the mean Spearman correlation coefficient ρ_{Sp} for ordinal rating data. The association strength of the characteristics with respect to binary clinical factors (blue columns) was measured as the AUC and the p-values of Mann-Whitney U tests for the per-class differences. Spearman coefficient ρ_{Sp} correlates morphological attribute and the clinical factor (red columns), along with its p-value. Single asterisk, double asterisks, and triple asterisks indicate significance at the $\alpha = 0.05$, 0.01, and 0.001 level, under consideration of the Bonferroni correction, all significant associations are shaded in yellow

Characteristic	Data / Sample	RF	Agreem.	Rupture 78 unruptured 41 ruptured 119 total AUC	p-val	Sex 36 male 98 female 134 total AUC	p-val	Smoking 40 non-smokers 74 smokers 114 total AUC	p-val	Hypertension 70 non-hypertens. 49 hypertensive 119 total AUC	p-val	IA size (aSz) 134 aneurysms Mean: 6.9mm Std: 3.4mm ρ_{Sp}	p-val	Patient age 104 aneurysms Mean: 53.0y Std: 12.1y ρ_{Sp}	p-val
Rough surface	26 raters	0.21	κ 0.66	0.59	0.12	0.55	0.41	0.51	0.90	0.50	0.97	0.68	***	0.03	0.76
Blebs	26 raters	0.43	κ 0.63	0.71	**	0.54	0.53	0.56	0.32	0.52	0.70	0.50	***	0.10	0.33
Lobules	26 raters	0.31	κ 0.65	0.79	***	0.64	0.01	0.52	0.68	0.52	0.69	0.40	**	0.02	0.83
Asymmetry	26 raters	0.47	κ 0.54	0.81	***	0.59	0.10	0.51	0.85	0.53	0.62	0.49	***	0.09	0.39
Complex vasc.	26 raters	0.17	κ 0.52	0.51	0.85	0.56	0.28	0.52	0.76	0.57	0.17	0.13	0.28	0.03	0.76
Irregularity	39 raters	-	ρ_{Sp} 0.84	0.81	***	0.58	0.14	0.50	0.90	0.51	0.79	0.71	***	0.08	0.42
Aneurysm size	134 IAs	-	-	0.71	**	0.62	0.03	0.57	0.18	0.52	0.24	-	-	0.14	0.16
Non-sphericity	134 IAs	-	-	0.83	***	0.60	0.07	0.55	0.38	0.50	0.97	0.61	***	0.01	0.93
Curvature	134 IAs	-	-	0.78	***	0.58	0.15	0.55	0.34	0.52	0.78	0.81	***	0.09	0.38
Patient age	110 pats	-	-	0.58	0.21	0.59	0.18	0.55	0.48	0.74	*	0.14	0.16	-	-

of determination (R^2) and the root mean square error (RMSE) as performance metrics, averaged over 100 randomly shuffled re-instantiations of our dataset of ratings (mean and standard deviation of total 500 samples). Finally, we expanded the multivariate regression model by quantitative metrics such as aSz, NSI, and GLN to examine if the proposed set of morphological attributes possibly requires extension.

Relationship between morphology and clinical factors

We examined the aggregated ratings of morphological characteristics for a relationship with the following clinically relevant factors: (i) for the aneurysm: rupture status, size, and location; (ii) for the patient: sex, age, history of smoking (former or current smoker), history of hypertension (patient with treated or untreated hypertension).

For *continuous* variables (aneurysm size and patient age), we report Spearman rank correlation coefficients between these variables and the aggregated ratings. For *binary* parameters (rupture status, sex, smoking status, and history of hypertension), we computed univariate classification models (logistic regression, 5-fold cross-validated, 100 data shuffles). The area under the receiver operating characteristic curve (AUC) served as a primary performance measure. We report the mean and standard deviation over all 500 re-instantiations of the test dataset: AUC = mean ± std. Additionally, we tested the per-class differences for statistical significance using two-sided Mann-Whitney U tests (significance level $\alpha = 0.05$). We applied conservative Bonferroni correction for multiple pairwise testing, for which we set the correction factor to 60 (four binary and two continuous parameters times 10 characteristics to be examined).

To assess *location dependency*, we restricted the analysis to locations with at least 20 samples: the M1 segment of the middle cerebral artery (MCA M1), ophthalmic segment of the internal carotid artery (ICA oph), and aneurysms at the posterior and anterior communicating artery (PComA and AComA). These locations cover 73% of the cases (Table 1).

We computed *multivariate* classification models (logistic regression) to examine the relationship between morphology and rupture status, combining perceived irregularity with morphometrics (aSz, NSI, GLN) and location. One-hot encoding was used to represent categorical variables (location) in a metric feature space. We applied the same model validation scheme as for the univariate case.

Results

Rating data

We investigated the consistency among the raters and between experts and laypersons for both irregularity and morphological attributes. This ensures that the aggregated metrics represent the collective opinion sufficiently well. The rating data comprised of 5219 ordinal irregularity ratings (39 raters, 134

cases, 7 misses) and 17,420 binary ratings (26 raters, 134 cases, 5 attributes, 0 misses).

Perceived irregularity The individual orderings of the cases by increasing irregularity rating agree well with the collective opinion on irregularity, indicated by a mean Spearman correlation coefficient of $\rho_{Sp} = 0.84$ ($p < 0.001$) between the absolute ratings and perceived irregularity. On an absolute scale, clinical experts rated the cases significantly higher than instructed laypersons by 0.47 (paired-sample t-test, $p < 0.001$, $n = 134$). The distributions of ratings were more consistent within clinical raters (indicated by a narrow interquartile range for the mean ratings per raters in Fig. 1a). However, the rater agreement per case (measured as the standard deviation of ratings) was similar for both clinicians and laypersons (paired-sample t-test, $p = 0.89$, $n = 134$). Also, the rater subcohorts cannot be discriminated statistically if the bias-adjusted (ranked) metric *perceived irregularity* is used (paired-sample t-test, $p = 0.97$; Fig. 1c).

Perceived morphological attributes Based on the mean Cohen's κ between raters and the binarized average rater, we observe substantial rater agreement for the assessment of rough surface, blebs, and lobules, and moderate-to-substantial agreement for asymmetry and complex vasculature (Table 2). Again, no statistically significant difference in the bias-adjusted agreement metric was identified between clinical experts and instructed laypersons. The rating aggregates are illustrated for a selection of aneurysms in Table 3.

Relationship with quantitative metrics We measured Spearman correlation coefficients ρ_{Sp} of 0.70, 0.80, and 0.89

between perceived irregularity and the quantitative metrics aSz, NSI, and GLN, respectively (Table 4).

Relationship between morphological attributes and irregularity

The univariate relationships between perceived irregularity and the five morphological attributes are illustrated in Fig. 2. The multifactorial linear model combining all morphological attributes revealed $R^2 = 0.92 \pm 0.03$ and RMSE $= 0.075 \pm 0.011$ for a total of 100 re-evaluations (5-fold cross-validation, 20 repetitions). Adding NSI as a factor improved the model accuracy significantly: $R^2 = 0.95 \pm 0.02$, RMSE $= 0.061 \pm 0.008$ (see Fig. 3a). Expanding the quantitative metrics for aneurysm size (aSz) and curvature (GLN) did not improve the model further. Examining different classes of morphometrics (geometry features [28], writhe-based features [19], Zernike moment invariants [24]), we observed that metrics measuring dome *elongation* (NSI, ellipticity index, aspect ratio [28]) improved the model accuracy the best.

Relationship between morphology and clinical factors

Rupture status Of the 119 aneurysms with known rupture status, 41 were ruptured and 78 unruptured. The average irregularity rating ranks were significantly higher for ruptured aneurysms (two-sided Mann-Whitney U test, $p < 0.001$). This observation held true also if the data was stratified by the two rater groups. To assess the discriminative capability of perceived irregularity, we visualized the ratio of ruptured versus unruptured cases as a function of perceived irregularity for a sliding window (width 0.2; Fig. 3b). We also computed the mean AUC to be 0.81 ± 0.04. For the optimal point of the mean receiver operating characteristic (ROC) curve, this translates to a model accuracy of 0.74 (sensitivity 0.73, specificity 0.74). Besides overall perceived irregularity, we were able to find strong associations between perceived asymmetry, as well as perceived presence of blebs and lobules, aneurysm size (aSz), and non-sphericity (NSI) (see Fig. 3b, c and Table 2). A multivariate logistic regression model combining perceived irregularity, aSz, and NSI outperformed the univariate model in terms of mean AUC (0.82 ± 0.08), but the difference did not reach statistical significance (unpaired Student's t-test, $p = 0.13$). Combining irregularity with (one-hot encoded) location predictors, on the other hand, significantly increased the AUC to 0.87 ± 0.09 (unpaired Student's t-test, $p < 0.001$). In this model, we considered only the four locations with at least 20 samples (MCA M1, ICA oph, PComA, and AComA).

Patient sex, smoking history, history of hypertension, and age Neither perceived irregularity nor any of the five
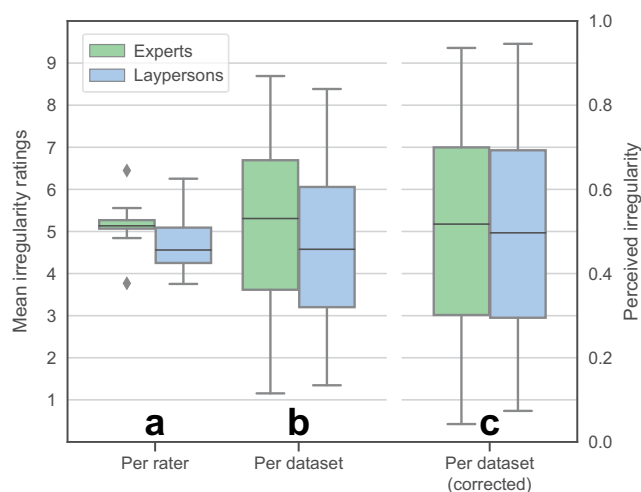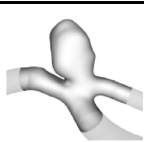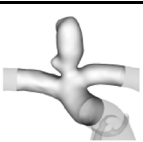

Fig. 1 Rating characteristics stratified by cohort. **a** and **b** visualize the mean absolute ratings per rater and per dataset, respectively. **c** shows the same data as **b** after correcting for rater bias: mean of ranked ratings, normalized to the range [0,1]

Table 3 Selected IAs and their qualitative and quantitative characteristics. The cases are sorted from left to right by increasing perceived irregularity. *AComA*, anterior communicating artery; *aSz*, aneurysm size; *BA tip*, tip of the basilar artery; *ICA bif*, ICA bifurcation; *MCA M1*, M1 segment of the middle cerebral artery; *NSI*, non-sphericity index; *PICA*, posterior inferior cerebellar artery

Aneurysm	MCA M1 unruptured	ICA bif unruptured	PICA ruptured	ICA bif unruptured	BA tip ruptured	AComA unruptured	AComA ruptured
Patient	female, 54y	male, 40y	female, 42y	female, 24y	female, 66y	female, 62y	male, 78y
Irregularity	0.08	0.41	0.60	0.79	0.81	0.87	0.93
Rough surf.	0.00	0.32	0.16	0.16	0.24	0.68	0.08
Blebs	0.04	0.33	0.50	0.96	0.83	1.00	0.92
Lobules	0.00	0.08	0.40	0.16	0.44	0.24	0.64
Asymmetry	0.12	0.40	0.56	0.48	0.68	0.52	0.92
Vasculature	0.27	0.04	0.00	0.04	0.46	0.15	0.15
NSI	0.05	0.21	0.18	0.27	0.12	0.16	0.26
aSz [mm]	3.14	6.88	5.50	7.11	6.29	9.49	8.39

morphological attributes considered in this study carried significant information on patient sex, smoking status, or hypertension (Table 2). Likewise, the analysis of the (Spearman) correlation between age and morphological characteristics did not reveal any statistically significant association. Male patients develop aneurysms with larger aSz and NSI, and with lobules being perceived more likely, but the observation did not reach statistical significance (Table 2).

Aneurysm location Unruptured MCA M1 aneurysms tended to be more asymmetric than unruptured IAs of the other three locations. Likewise, unruptured ICA oph IAs were perceived as considerably more regular, exhibiting fewer blebs/lobules and, possibly related, a lower NSI than the rest of the unruptured cases. Note that in our dataset, the ICA oph and MCA M1 aneurysms exhibited a relatively strong imbalance between ruptured and unruptured IAs (rupture ratio 1:5), while for PComA and AComA IAs, the rupture ratio was nearly balanced.

Table 4 Spearman correlation coefficients ρ_{Sp} between the six morphological characteristics examined in this study and the metrics for aneurysm size (aSz), non-sphericity/elongation (NSI), and total Gaussian curvature (GLN). The color maps values between 0 (red) and 1 (green)

	aSz	NSI	GLN
irregularity	0.70	0.80	0.89
asymmetry	0.47	0.73	0.71
rough surface	0.65	0.22	0.49
blebs	0.51	0.56	0.72
lobules	0.41	0.70	0.65
vasculature	0.13	-0.13	-0.01

Discussion

Shape assessments of clinical experts (neurosurgeons, interventional neuroradiologists) and instructed laypersons are statistically indistinguishable in terms of relative ordering of the cases. This suggests that the assessment of IA morphology with our experimental setup is guided by the intuitive, visual perception of geometry rather than prior knowledge about the disease. With regard to the observed difference of average irregularity ratings, we conjecture that clinicians rely on an individual mental model covering a wider spectrum of cases than the dataset included in this study.

Overall, we found good agreement of the raters with the collective aggregates for perceived irregularity and morphological attributes. The observed variability in the rating data is a consequence of the open task formulation, the inconsistency typical for human subjective assessment (perceptual and attentional differences), the heterogeneous composition of the rater cohort, and the number of rating levels. We measured a moderate-to-substantial interrater agreement for morphological attributes, comparable with Suh et al. [30] for the human discrimination of daughter sacs and lobulations.

We modeled perceived irregularity by means of all morphological attributes using multivariate linear regression. By considering the attributes asymmetry, rough surface, blebs, lobules, and complex parent vasculature, the perceived irregularity was explained already very accurately. This suggests that our rater cohort was inherently consistent with its ratings for irregularity and morphological attributes, and that our particular choice of morphological attributes reflects the various manifestations of perceived irregularity reasonably. Extending the regression model by quantitative metrics for size and morphology allowed us to identify elongation/non-
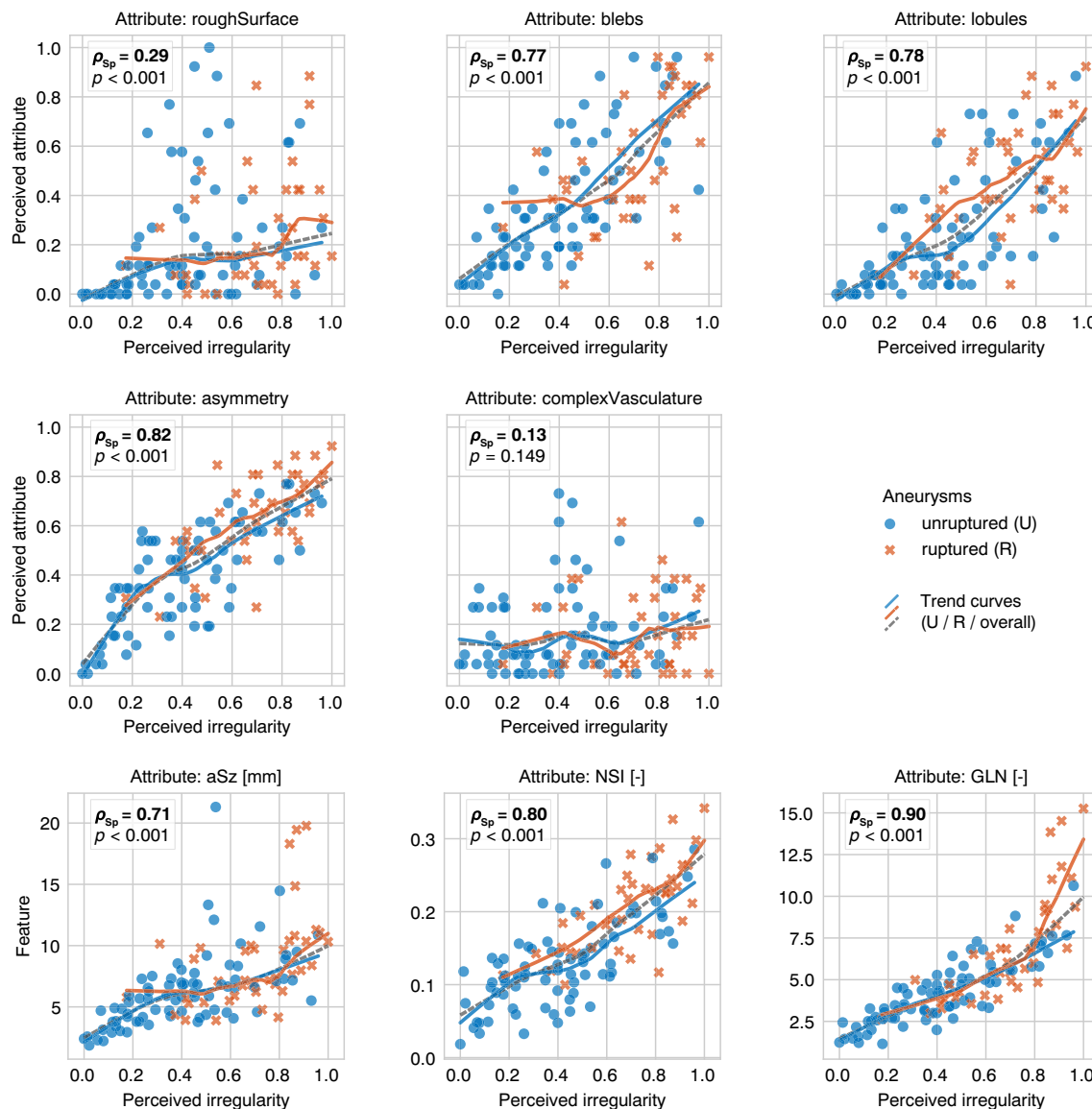
Fig. 2 Perceived irregularity in relation with morphological characteristics (rough surface, presence of blebs or lobules, asymmetry, or complex vasculature) and selected quantitative features (aSz, aneurysm size; NSI, non-sphericity index; GLN, total Gaussian curvature). The colors/markers encode the rupture status, interpolation curves indicate trends. The Spearman correlation coefficients ρ_{Sp} and the corresponding p-values are also provided

sphericity as a sixth characteristic, which we had not considered a priori as a rating attribute.

The model predicting perceived irregularity by means of the measurements of the morphological attributes ($R^2 = 0.95 \pm 0.02$) outperforms our model based on quantitative features considerably ($R^2 = 0.84 \pm 0.05$; see [13]). This suggests that our set of quantitative features was not comprehensive enough to capture the human perception with sufficient accuracy and requires further extension.

The regression model links morphological attributes to perceived irregularity. Its coefficients (Table 5) can be interpreted by how much the presence of a morphological trait contributed to the average rater's perception of irregularity. Note that the different morphological attributes were not equally

prevalent in our dataset. Complex parent vasculature or rough surface was identified only half as frequently as the presence of blebs or asymmetry (Table 2).

From the clinical risk factors considered, only aneurysm size was linked to morphology, which reflects the well-established fact that pathogenic wall processes stimulate both global growth of the aneurysm and the formation of morphological structure. [2, 12, 23] We found no association of morphology with patient sex and age, although these factors play a role in the prevalence of aneurysms. [32]. The same holds for smoking, which is known to have an adverse effect on the vessel wall integrity and aneurysm formation and growth. [14]

Perceived irregularity spanned a continuum that is strongly linked to rupture status. With higher irregularity, the rupture
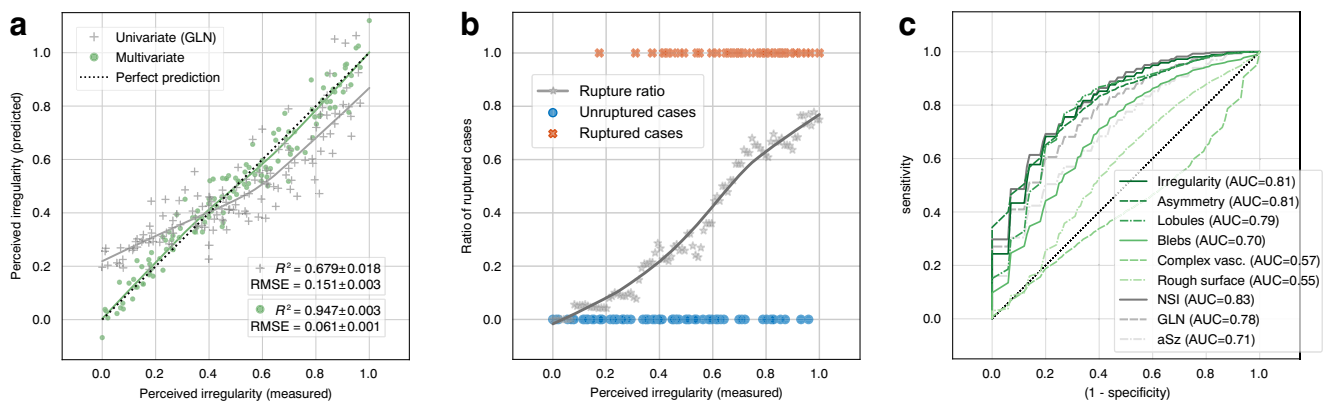
Fig. 3 **a** Perceived irregularity measured for the 134 aneurysms in relation with the irregularity reproduced by a univariate linear regression model based on curvature index GLN and a multivariate linear regression based on six predictors: asymmetry, rough surface, blebs, lobules, complex vasculature, and non-sphericity (NSI). Interpolation curves indicate trends. **b** Relationship between perceived irregularity and rupture. The ratio of ruptured aneurysms is computed in a sliding window of width 0.2 for perceived irregularity (gray markers and trendline). The rupture status of each case is marked (blue and red markers). **c** Mean receiver operating characteristic (ROC) curves illustrate the ability of the morphological characteristics considered to discriminate the aneurysm rupture status. A larger area under the curve (AUC) signifies higher discriminative power. R^2, coefficient of determination; RMSE, root mean square error; aSz, aneurysm size

ratio increased (Fig. 3b). Irregularity alone discriminated ruptured from unruptured aneurysms relatively accurately (AUC 0.81, prediction accuracy 0.73). Combining perceived irregularity with location increased the association significantly (AUC 0.87, prediction accuracy 0.78), which confirms the widely accepted view that aneurysm morphology varies with location. The performance of our two-factor model (perceived irregularity, aneurysm location) was comparable with recent multifactorial models for aneurysm rupture status [5, 8, 21, 35, 36].

We compared our results with the findings reported by Lindgren et al. [20], where the shape irregularity of 5814 aneurysms was rated on a binary scale (single assessments only). For this, we binarized our irregularity ratings using the optimal ROC point (optimality based on Youden's J statistic), resulting in 73% of the ruptured aneurysms and 26% of the unruptured aneurysms being classified as irregular, which is in good agreement with the corresponding rates of 92% and 22% reported by [20]. The difference can possibly be

explained by the fact that stable aneurysms with a regular shape are underrepresented in our dataset, and that irregular structures are more easily perceived in 3DRA images than in MR or CT angiograms.

Aneurysm shape may change under rupture in some cases. [20, 29] To examine whether the rater assessment varies with rupture status, we re-evaluated our study on the subset of unruptured aneurysms alone and were able to reproduce our key observations that raters assess irregularity consistently ($\rho_{Sp} = 0.81$ vs. $\rho_{Sp} = 0.84$ for the complete dataset) and that irregularity is decoded by morphological attributes (AUC for multivariate linear regression model 0.94 ± 0.03, compared with 0.95 ± 0.02). From this, we conclude that the assessment of morphology is independent of the rupture status. Unruptured IAs still exhibited variations in morphological characteristics, albeit to a lesser extent than ruptured aneurysms. This confirms the prevailing view that morphological structures develop gradually as a result of complex processes within the wall and therefore primarily reflect the stability of the lesion rather than the rupture event itself.

Limitations

3DRA data tend to be biased towards unstable cases. The inclusion of patients with multiple aneurysms (21 out of 110 patients) mitigates this limitation slightly because secondary aneurysms tend to have simpler geometries. Using MR or CT angiographic data would solve this problem partially but demands higher efforts in image processing and standardization.

To simplify the qualitative and quantitative assessment of the aneurysm geometry, we operated with 3D surface models derived from 3DRA. We do not see any obstacles to applying

Table 5 Coefficients of the multivariate linear regression model for perceived irregularity including the five morphological attributes plus dome elongation, averaged over 100 repeated model evaluations (mean ± std)

Attribute	Coefficient
Intercept	$c_0 = -0.09 \pm 0.01$
Asymmetry	$c_1 = 0.12 \pm 0.02$
Rough surface	$c_2 = 0.28 \pm 0.01$
Blebs	$c_3 = 0.34 \pm 0.01$
Lobules	$c_4 = 0.38 \pm 0.02$
Complex vasculature	$c_5 = 0.28 \pm 0.02$
Non-sphericity/elongation	$c_6 = 0.30 \pm 0.02$

the suggested rating scheme on 3D medical imaging data directly, without the detour of extracting 3D surfaces.

The collocation of morphological attributes and pathological intramural processes or thrombus formation has not been addressed in this study, but concepts exist how to relate morphological with wall histological data [7, 25].

Conclusions

We showed that perceived irregularity of the lumen can be decomposed consistently into six different morphological attributes that reflect remodeling processes of the aneurysmal wall: presence of a rough surface, blebs, lobules, asymmetry, an elongated dome, and a complex geometry of the parent vasculature.

Morphology carries important information on the disease status of IAs. Perceived irregularity, asymmetry, the presence of lobules, and, to a lower extent, blebs, are more frequent in ruptured aneurysm. Our association model for rupture status based solely on aneurysm morphology and location achieves similar discrimination performance compared with recent studies but requires considerably fewer factors.

With the curvature metric GLN, and, to a slightly lower extent, non-sphericity NSI, being well correlated with perceived irregularity, these indices can be considered first-order quantitative proxies for morphological irregularity.

Irregularity is independent from the clinical factors patient sex, age, history of smoking, and hypertension. In contrast, aneurysm location and size have a significant impact on morphology. In particular the location dependency deserves further attention.

IAs constitute a vessel wall pathology that shows a great variability, which is also reflected in the shape. Structural wall heterogeneity is associated with morphological irregularity. The assessment of morphology from vessel lumen holds the potential for an automated shape analysis that establishes irregularity as a biomarker for vessel wall instability.

Compliance with ethical standards

Conflict of interest The authors declare that they have no conflict of interest.

Ethical approval All procedures performed in studies involving patients were in accordance with the ethical standards of the institutional and/or national research committee and with the 1964 Helsinki declaration and its later amendments or comparable ethical standards. Raw 3D-DRA of the AneuX test data set were provided by the University Hospital of Geneva and collected with formal patient consent according to the @neurIST protocol and ethics authorization PB_2018-00073 (previously CER 07-05) released June 1st 2007 and renewed April 13th 2010, August 19th 2014, and February 28th 2018 initially by the Geneva Cantonal Ethics Commission for Research involving Humans and renewed by Swissethics in 2018.

References

1. Backes D, Rinkel GJE, Greving JP et al (2017) ELAPSS score for prediction of risk of growth of unruptured intracranial aneurysms. Neurology 88(17):1600–1606
2. Beck J, Rohde S, El Beltagy M, Zimmermann M, Berkefeld J, Seifert V, Raabe A, Mura JM, Rojas-Zalazar D, De Oliveira E (2003) Difference in configuration of ruptured and unruptured intracranial aneurysms determined by biplanar digital subtraction angiography. Acta Neurochir 145(10):861–865
3. Berkowitz BM (2016) Development of metrics to describe cerebral aneurysm morphology. University of Iowa
4. Bijlenga P, Ebeling C, Jaegersberg M et al (2013) Risk of rupture of small anterior communicating artery aneurysms is similar to posterior circulation aneurysms. Stroke 44(11):3018–3026
5. Bisbal J, Engelbrecht G, Villa-Uriol MC, Frangi AF (2011) Prediction of cerebral aneurysm rupture using hemodynamic, morphologic and clinical features: a data mining approach. Lect Notes Comput Sci (including Subser Lect Notes Artif Intell Lect Notes Bioinformatics) 6861 LNCS(PART 2):59–73
6. Bogunović H, Pozo JM, Villa-Uriol MC, Majoie CBLM, van den Berg R, Gratama van Andel HAF, Macho JM, Blasco J, San Román L, Frangi AF (2010) Automated segmentation of cerebral vasculature with aneurysms in 3DRA and TOF-MRA using geodesic active regions: an evaluation study. Med Phys 38(1):210–222
7. Cebral J, Ollikainen E, Chung BJ, Mut F, Sippola V, Jahromi BR, Tulamo R, Hernesniemi J, Niemelä M, Robertson A, Frösen J (2017) Flow conditions in the intracranial aneurysm lumen are associated with inflammation and degenerative changes of the aneurysm wall. Am J Neuroradiol 38(1):119–126.
8. Detmer FJ, Chung BJ, Mut F, Slawski M, Hamzei-Sichani F, Putman C, Jiménez C, Cebral JR (2018) Development and internal validation of an aneurysm rupture probability model based on patient characteristics and aneurysm location, morphology, and hemodynamics. Int J Comput Assist Radiol Surg. https://doi.org/10.1007/s11548-018-1837-0
9. Dhar S, Tremmel M, Mocco J, Kim M, Yamamoto J, Siddiqui AH, Hopkins LN, Meng H (2008) Morphology parameters for intracranial aneurysm rupture risk assessment. Neurosurgery 63(2):185–196
10. Etminan N, Brown RD, Beseoglu K, et al (2015) The unruptured intracranial aneurysm treatment score. Neurology 85(10):881–889
11. Forbes G, Fox AJ, Huston III J, Wiebers DO, Torner J (1996) Interobserver variability in angiographic measurement and morphologic characterization of intracranial aneurysms: a report from the International Study of Unruptured Intracranial Aneurysms

12. Frösen J, Tulamo R, Paetau A, Laaksamo E, Korja M, Laakso A, Niemelä M, Hernesniemi J (2012) Saccular intracranial aneurysm: pathology and mechanisms. Acta Neuropathol 123(6):773–786

13. Juchler N, Schilling S, Glüge S, Bijlenga P, Rüfenacht D, Kurtcuoglu V, Hirsch S (2020) Radiomics approach to quantify shape irregularity from crowd-based qualitative assessment of intracranial aneurysms. Computer Methods in Biomechanics and Biomedical Engineering: Imaging and Visualization. https://doi.org/10.1080/21681163.2020.1728579

14. Juvela S, Porras M, Poussa K (2000) Natural history of unruptured intracranial aneurysms: probability of and risk factors for aneurysm rupture. J Neurosurg 93(3):379–387

15. Karamanakos PN, Von Und Zu Fraunberg M, Bendel S, Huttunen T, Kurki M, Hernesniemi J, Ronkainen A, Rinne J, Jaaskelainen JE, Koivisto T (2012) Risk factors for three phases of 12-month mortality in 1657 patients from a defined population after acute aneurysmal subarachnoid hemorrhage. World Neurosurg 78(6):631–639

16. Kleinloog R, De Mul N, Post JA, Rinkel GJE (2017) Risk factors for intracranial aneurysm rupture: a systematic review. Neurosurgery 82(4):431–440

17. Krings T, Mandell DM, Kiehl TR, Geibprasert S, Tymianski M, Alvarez H, TerBrugge KG, Hans FJ (2011) Intracranial aneurysms: from vessel wall pathology to therapeutic approach. Nat Rev Neurol 7(10):547–559

18. Larrabide I, Omedas P, Martelli Y, et al (2009) GIMIAS: an open source framework for efficient development of research tools and clinical prototypes. Lect Notes Comput Sci (including Subser Lect Notes Artif Intell Lect Notes Bioinformatics) 5528:417–426

19. Lauric A, Miller EL, Baharoglu MI, Malek AM (2011) 3D shape analysis of intracranial aneurysms using the writhe number as a discriminant for rupture. Ann Biomed Eng 39(5):1457–1469

20. Lindgren AE, Koivisto T, Björkman J, von und zu Fraunberg M, Helin K, Jääskeläinen JE, Frösen J (2016) Irregular shape of intracranial aneurysm indicates rupture risk irrespective of size in a population-based cohort. Stroke 47:1219–1226

21. Liu Q, Jiang P, Jiang Y, Ge H, Li S, Jin H, Li Y (2019) Prediction of aneurysm stability using a machine learning model based on PyRadiomics-derived morphological features. Stroke 50(9):2314–2321

22. Ma B, Harbaugh RE, Raghavan ML (2004) Three-dimensional geometrical characterization of cerebral aneurysms. Ann Biomed Eng 32(2):264–273

23. Meng H, Tutino VM, Xiang J, Siddiqui A (2014) High WSS or low WSS? Complex interactions of hemodynamics with intracranial aneurysm initiation, growth, and rupture: toward a unifying hypothesis. Am J Neuroradiol 35(7):1254–1262

24. Millan RD, Dempere-Marco L, Pozo JM, Cebral JR, Frangi AF (2007) Morphological characterization of intracranial aneurysms using 3-D moment invariants. IEEE Trans Med Imaging 26(9):1270–1282

25. Morel S, Diagbouga MR, Dupuy N et al (2018) Correlating clinical risk factors and histological features in ruptured and unruptured human intracranial aneurysms: the Swiss AneuX Study. J Neuropathol Exp Neurol 77(7):555–566

26. Nieuwkamp DJ, Setz LE, Algra A, Linn FH, de Rooij NK, Rinkel GJ (2009) Changes in case fatality of aneurysmal subarachnoid haemorrhage over time, according to age, sex, and region: a meta-analysis. Lancet Neurol 8(7):635–642

27. Piccinelli M (2012) Characterization of cerebral aneurysm morphology: development of methods and techniques in an open-source framework. Technische Universiteit Eindhoven. https://doi.org/10.6100/IR741500

28. Raghavan ML, Ma B, Harbaugh RE (2005) Quantified aneurysm shape and rupture risk. J Neurosurg 102(2):355–362

29. Schneiders JJ, Marquering HA, Van Den Berg R, VanBavel E, Velthuis B, Rinkel GJE, Majoie CB (2014) Rupture-associated changes of cerebral aneurysm geometry: high-resolution 3D imaging before and after rupture. Am J Neuroradiol 35(7):1358–1362

30. Suh SH, Cloft HJ, Huston J, Han KH, Kallmes DF (2014) Interobserver variability of aneurysm morphology: discrimination of the daughter sac. J Neurointerv Surg 8(1):38–41

31. Japan Investigators UCAS (2012) The natural course of unruptured cerebral aneurysms in a Japanese cohort. N Engl J Med 366:2474–2482

32. Vlak MHM, Algra A, Brandenburg R, Rinkel GJE (2011) Prevalence of unruptured intracranial aneurysms, with emphasis on sex, age, comorbidity, country, and time period: a systematic review and meta-analysis. Lancet Neurol 10(7):626–636

33. Wanke I, Rüfenacht DA (2017) Zufallsbefund intrakranielles Aneurysma. Swiss Medical Forum 17(4):80–82

34. Wermer MJH, Van Der Schaaf IC, Algra A, Rinkel GJE (2007) Risk of rupture of unruptured intracranial aneurysms in relation to patient and aneurysm characteristics: an updated meta-analysis. Stroke 38(4):1404–1410

35. Xiang J, Natarajan SK, Tremmel M, Ma D, Mocco J, Hopkins LN, Siddiqui AH, Levy EI, Meng H (2011) Hemodynamic-morphologic discriminants for intracranial aneurysm rupture. Stroke 42(1):144–152

36. Xiang J, Yu J, Snyder KV, Levy EI, Siddiqui AH, Meng H (2016) Hemodynamic-morphological discriminant models for intracranial aneurysm rupture remain stable with increasing sample size. Journal of Neurointerventional Surgery 8(1):104–110